Reconstitution of Kinetochore and Microtubule Dynamics Reveals a Role for a Kinesin-8 in Establishing End-on Attachments

Julia R. Torvi [1,2]*, **Jonathan Wong** [1]*, **Daniel Serwas** [1], **Amir Moayed**[1], **David G. Drubin** [1,2], and **Georjana Barnes** [1]✉

*These authors contributed equally to this work
[1]Department of Molecular and Cell Biology, University of California, Berkeley, CA 94720, USA
[2]Biophysics Graduate Group, University of California, Berkeley, CA 94720, USA

During mitosis, individual microtubules make attachments to chromosomes via a specialized protein complex called the kinetochore to faithfully segregate the chromosomes to daughter cells. Translocation of kinetochores on the lateral surface of the microtubule has been proposed to contribute to high fidelity chromosome capture and alignment at the mitotic midzone, but has been difficult to observe *in vivo* because of spatial and temporal constraints. To overcome these barriers, we used total internal reflection fluorescence (TIRF) microscopy to track the interactions between endogenously tagged tubulin, kinetochore proteins, and other microtubule-associated proteins in lysates from metaphase-arrested *Saccharomyces cerevisiae*. Using both TIRF microscopy and cryo-correlative light microscopy and electron tomography, we successfully reconstituted microtubule-bound, intact kinetochores. These kinetochores translocate on the lateral microtubule surface toward the microtubule plus end and transition to end-on attachment, whereupon microtubule depolymerization commences. The directional kinetochore movement is dependent on the highly processive kinesin-8, Kip3. We propose that Kip3 facilitates stable kinetochore attachment to microtubule plus ends through its abilities to move the kinetochore laterally on the surface of the microtubule and to regulate microtubule plus end dynamics.

Introduction

During mitosis, a cell's replicated chromosomes are equally segregated to two daughter cells. In order for this process to happen accurately and efficiently, the microtubule cytoskeleton must completely remodel to form a bipolar spindle. Replicated chromosomes then attach to microtubules, emanating from opposite spindle poles, through a large dynamic chromosome-associated protein complex called the kinetochore. Proper kinetochore-microtubule attachment is vital for preservation of genomic integrity and prevention of cancer and birth defects (Weaver and Cleveland, 2005). Therefore, kinetochore attachment is highly regulated and tightly controlled (Tanaka, 2013).

During establishment of biorientation, kinetochores have been observed to first attach to the lateral surface of a microtubule (Tanaka, 2012). Such kinetochores then must be transported along the microtubule lattice, where they transition to an appropriate, and stable, end-on attachment (Rieder and Alexander, 1990; Tanaka et al., 2005; Kapoor et al., 2006). It is only after each sister kinetochore makes a proper end-on attachment with microtubules from opposite spindle poles that the cell will progress into anaphase and complete mitosis. This lateral to end-on attachment conversion has been

observed in several eukaryotic species (Magidson et al., 2015; Maiato et al., 2017), but the underlying mechanisms have been elusive due both to the difficulty of observing this event *in vivo* and to biochemical hurdles *in vitro*.

Establishment of end-on kinetochore attachments to microtubules, for chromosomes that are initially attached to spindle microtubules laterally, can be divided into two processes: (1) chromosome lateral movement along the microtubule surface, and (2) conversion from lateral to end-on attachment. With regard to the kinetochore reaching the microtubule tip, CENP-E and chromokinesins are particularly important for chromosome movement to the spindle midzone in metazoans (Craske and Welburn, 2020; Lemura and Tanaka, 2015). However, fungi do not appear to have kinesin-7 or chromokinesin orthologs. Lateral to end-on conversion has been observed in fungi, but these events required that a depolymerizing microtubule tip meet the laterally bound kinetochore (Kalantzaki et al., 2015). Other studies in fungi have also implicated minus-end directed motor-based transport of unattached kinetochores (Tanaka et al., 2005), similar to a proposed metazoan mechanism involving the motor protein dynein and the mitotic spindle protein NuMA (Kapoor et al., 2006; Li et al., 2007).

One class of proteins that might be involved in lateral kinetochore movements is the kinesin-8 motor proteins. This family of proteins includes key regulators of kinetochore-microtubule dynamics that increase microtubule rescue and catastrophe frequencies, thus tuning microtubule dynamics for proper chromosome segregation (Risteski et al., 2021). In budding yeast, Kip3, a highly processive kinesin-8, is required for kinetochore clustering into two discrete foci at metaphase, but how this activity relates to establishment of end-on attachments is not clear (Wargacki et al., 2010; Su et al., 2011). Declustered kinetochores may represent misaligned or defectively attached chromosomes (Wargacki et al., 2010; Edzuka and Goshima, 2019; Shimogawa et al., 2010). Additionally, in yeast that lack Kip3, chromosomes lag behind the main chromosome mass during anaphase (Tytell and Sorger, 2006). The metazoan kinesin-8, Kif18a, is responsible for attenuating kinetochore-microtubule dynamics, which ultimately affects chromosome alignment and equal segregation into the daughter cells (Stumpff et al., 2008, 2012). Lagging chromosomes are common in cells lacking Kif18a and result in micronuclei formation (Fonseca et al., 2019). Additionally, the Drosophila kinesin-8, Klp67A, shares many of the roles of other kinesin-8 proteins including stabilizing and destabilizing microtubules, but this kinesin also stabilizes kinetochore-microtubule attachments (Edzuka and Goshima, 2019). Taken together, these observations indicate that kinesin-8 motor proteins have roles both in attenuating microtubule dynamics and in establishing kinetochore-microtubule attachments, while potentially playing a role in the formation of proper end-on attachments.

Currently, methods to observe single kinetochores trans-

ported along single microtubules are limited. An ideal assay would enable tracking of single intact kinetochores on microtubules assembled from tubulin isolated from the same species as those kinetochores; ideally a species with robust genetics so mutants could be used, and an assay that utilizes the full complexity of a cell. A cell-free system combines the full biochemical complexity of a cell with the experimental control provided by *in vitro* experiments. In this study, we investigated mitotic regulation of kinetochore-microtubule attachments and dynamics using a reconstitution system that employs cell cycle arrested extracts from the genetically tractable organism *Saccharomyces cerevisiae* (Bergman et al., 2018).

Results

Reconstitution of dynamic kinetochores on single yeast microtubules

To investigate the mechanism of kinetochore-microtubule attachment at metaphase, we sought to visualize single kinetochores on single microtubules. For these studies we employed a reconstitution assay wherein cell-cycle arrested whole cell yeast lysate was used to study regulation of microtubule dynamics (Bergman et al., 2018). Using this assay, we asked whether kinetochores and their dynamics could be observed by TIRF microscopy (Figure 1a). Fluorescently tagged kinetochore proteins from each of the major kinetochore subcomplexes were expressed at endogenous levels in strain backgrounds that also expressed fluorescently tagged alpha-tubulin (Tub1) and a temperature-sensitive allele (*cdc23-1*) of the gene that encodes a subunit of the anaphase-promoting complex, to arrest cells in metaphase at the non-permissive temperature (Irniger et al., 1995). The proteins we chose to tag spanned the entirety of the kinetochore (Figure 1b).

Outer kinetochore proteins are dynamic on microtubules

To begin, we tagged two outer kinetochore proteins known to bind to microtubules, Ndc80 (Cheeseman et al., 2006; Wei et al., 2007) and the Ask1 subunit of the Dam1 complex (Miranda et al., 2005; Westermann et al., 2005; Jenni and Harrison, 2018). Ndc80 and Ask1 kinetochore signals appeared on the microtubule surface (Figure 1c) and moved processively at an average rate of 0.56 µm/min toward the plus end of the microtubule (Figure 1d). Upon reaching the tip of the microtubule, Ndc80 and Ask1 appeared to transition irreversibly from lateral to end-on attachment. This end-on binding was then followed by microtubule depolymerization where Ndc80 and Ask1 tracked the depolymerizing microtubule end. The mean microtubule depolymerization rate also slowed from 0.82 µm/min (Bergman et al., 2018) to an average of 0.4 µm/min upon kinetochore binding to the microtubule tip (Figure 1d). After depolymerization onset, the microtubule was never observed to resume growth. Additionally, kinetochore proteins rarely, if ever, detached from the microtubule, either while bound laterally or to the microtubule tip. The directional switch of bound kinetochores was striking, as reflected in the dynamics of these kinetochore proteins and the percent of time the associated microtubules spent in the growing versus shrinking phase (Figure 1e). While laterally bound, kinetochores only move towards the plus end of the microtubule. When the kinetochore transitions from lateral to end-on attachment, the kinetochore only tracks the depolymerizing end of the microtubule and thus moves toward the minus-end of the microtubule.

In addition to the Ask1 movement that is the same as the Ndc80 movement: laterally along the MT toward the plus end mentioned above, we also observed a distinct Ask1 population that showed a unique behavior compared to other proteins assayed (Figure 1c). This Ask1 population was characterized by a very low intensity and diffuse signal, which briefly associated with and moved randomly along the microtubule. This signal was at the edge of the camera's detection limits and moved faster than our sampling rate. For these reasons, we did not investigate this Ask1 signal further. However, this observation potentially provides insight into Dam1 complex ring assembly and function on the microtubule (Gestaut et al., 2008; Grishchuk et al., 2008).

Inner kinetochore proteins are also dynamic on microtubules

We next tagged and assayed additional kinetochore proteins from the inner and middle kinetochore regions to determine their behaviors and to begin to assess whether all of the kinetochore proteins we observed associated with microtubules as intact kinetochore-like complexes. These additional labeled proteins included: Spc105, Mtw1 (MIND complex) Cnn1, Okp1 (COMA complex), Mif2, Ctf3 (CBF3 complex), and Cse4 (a centromeric histone variant) (Westermann et al., 2007; Biggins et al., 2013) (Figure 1b). Strikingly, for each kinetochore protein analyzed, we found dynamics similar to those we observed for Ask1 and Ndc80 (Figure 1c,d & e; Supplementary Movie SV1). These seven middle and inner kinetochore proteins have no known microtubule binding capabilities, implying that the kinetochore signals that we observed might represent intact or nearly intact kinetochores on microtubules in our assay.

Importantly, the kinetochore protein dynamics observed in metaphase-arrested cell lysates were specific to metaphase. When Spc105 dynamics were assayed in S-phase (*cdc7-1*) or anaphase (*cdc15-2*) arrested extracts (Goranov et al., 2009), the kinetochore proteins were stationary and did not move on the microtubule lattice (Figure S1a, b & c). Additionally, when Spc105 was observed at the microtubule tip, no tip-associated microtubule depolymerization occurred. Therefore, the kinetochore dynamics of the proteins shown in Figure 1 are specific to metaphase.
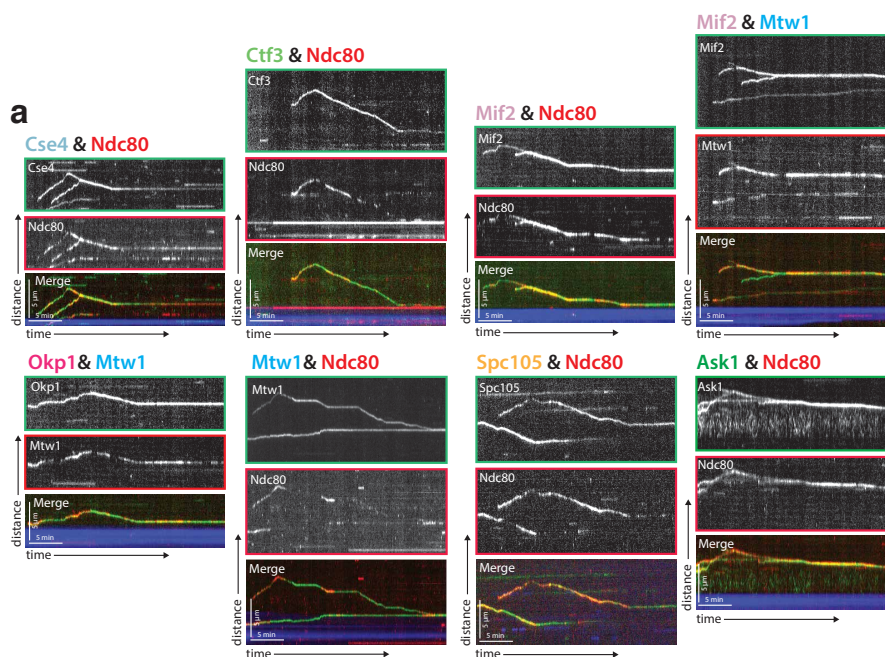
Kinetochore proteins from different sub-complexes move together on microtubules

The observation that inner kinetochore proteins (such as Cse4) which do not physically bind to microtubules, are in fact able to bind to and translocate on microtubules in our assay provided evidence that these kinetochore proteins were not alone or in small sub-complexes, but, in fact, were part of complete or nearly complete kinetochores. To explore this possibility further, we turned to dual-color imaging of kinetochore protein pairs and colocalization analyses. Due to its well-documented and canonical microtubule binding abilities, Ndc80 was chosen as a fiducial marker to which the localization of other kinetochore proteins was compared (Ciferri et al., 2007). One possibility was that proteins that reside further away from the Ndc80 complex would be less colocalized with it in our assay than proteins located closer to or adjacent to the Ncd80 complex (Figure 1b). On the contrary, when imaging different kinetochore proteins together with Ndc80, we, in fact, saw colocalization independent of that kinetochore protein's proximity to Ndc80 within the kinetochore (Figure 2; Supplement Movie SV2). Additionally, when using Mtw1, a more

Torvi, JR. & Wong, J. *et al.* | Reconstituted Kinetochore Dynamics
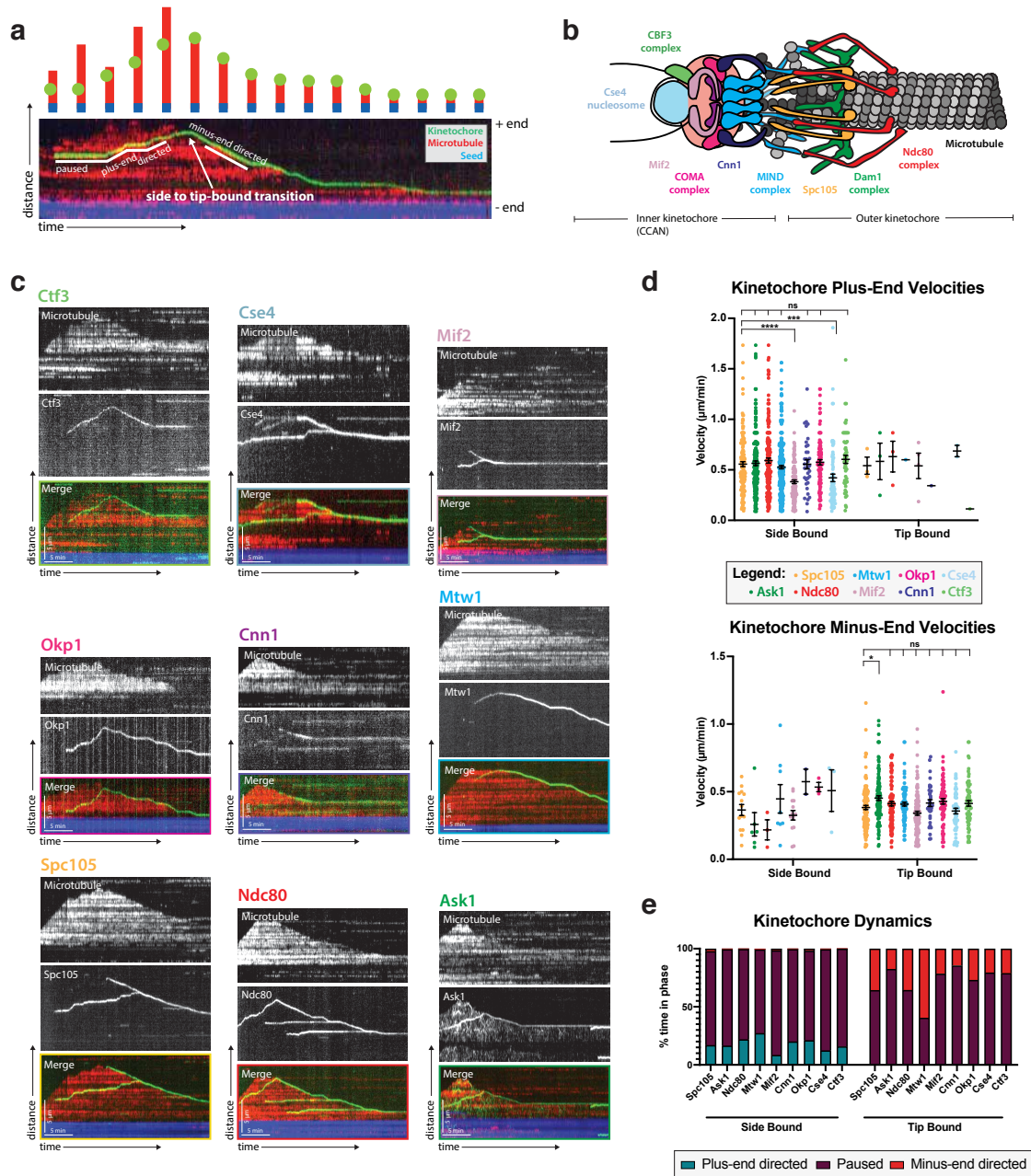
Figure 1. Kinetochore reconstitution and dynamics on the microtubule (**a**) Schematic of a typical kymograph representing a dynamic kinetochore on a microtubule. Time (min) is on the x-axis and distance (μm) is on the y-axis. Above the kymograph is a cartoon depiction explaining how the kymograph shows three-dimensional data in two-dimensional space. In both the kymograph and cartoon, the yeast microtubule is red, the kinetochore is green, and the porcine microtubule seed is blue. (**b**) A schematic of the budding yeast kinetochore with its major sub-complexes shown in different colors. These colors correspond to the different kinetochore proteins assayed in (c). The kinetochore is composed of inner kinetochore proteins such as the Cse4 nucleosome and the CBF3 complex, that bind to DNA, and outer kinetochore proteins such as the Ndc80 and Dam1 complex, that bind to the microtubule. (**c**) Reconstituted kinetochore proteins associated with yeast microtubules. Representative kymographs of kinetochore proteins from each sub-complex are shown. Time is on the x-axis and distance is on the y-axis (scale bars are 5 min and 5 μm, respectively). Kinetochore proteins are green and yeast microtubules are red. The porcine seed is blue. Each of the proteins assayed displays similar dynamics: moving toward the microtubule plus end when bound to the microtubule lateral surface. When the kinetochore proteins reach the plus end of the microtubule, they appear to convert from lateral to end-on attachment, which is often followed by microtubule depolymerization with the kinetochore remaining associated with the plus end. The microtubules were never observed to grow again following the depolymerization events in which a kinetochore protein was attached end-on. (**d**) Quantification of velocities and dynamics of kinetochores bound to microtubules. Kinetochores bound to the sides of microtubules move toward the microtubule plus end at an average velocity of 0.56 μm/minute. There were negligible minus-end directed movements when the kinetochore was side bound. When the kinetochores were associated with the microtubule tips, they tracked the microtubule tips as they depolymerized, moving at an average velocity of 0.4 μm/minute. There were also negligible plus-end directed movements when the kinetochore was bound to the tip. Each data point in the graph is the average velocity of one kinetochore. The error bars are the mean and standard error of the mean from 4 replicate trials of two biological replicates. Statistical analysis was done by a Kruskal-Wallis test where **** is P <0.0001, *** is P = 0.0003, and * is P = 0.0132. For the different kinetochore proteins: from Spc105 in order in the figure to Ctf3, N = 128, 155, 116, 102, 174, 56, 77, 59, 87 proteins tracked, respectively. (**e**) When the kinetochore is bound to the side of a microtubule, about 30% of its time it is in plus-end directed motion and the remaining 70% of the time it is paused (not moving). Kinetochores associated with plus ends spend 40% of the time moving toward the minus-end and 60% of the time paused.

Figure 2. Protein composition of reconstituted kinetochores Different pairwise combinations of kinetochore sub-complex proteins colocalize, establishing that the kinetochore spots observed by fluorescence microscopy are multi-protein, multi-subcomplex assemblies. Representative kymographs from each strain expressing a different pair-wise combination of tagged kinetochore proteins are shown. Time is on the x-axis and distance is on the y-axis (scale bars are 5 min and 5 μm, respectively). Ndc80 was used as the common reference marker for multiple pairwise combinations. Additionally, Mtw1 was used in some pairwise combinations to show that multiple sub-complexes are present in the same kinetochore. The tracks of these colocalized proteins follow similar dynamics as in Figure 1, where they move processively toward the microtubule plus end. At a certain point, they reach the plus end and motility becomes minus-end directed concomitant with the onset of microtubule disassembly (note that the microtubules are not visualized due to the inability to measure 4 colors, and the assumption is that this directional switch in kinetochore protein motility corresponds to microtubule depolymerization onset shown in Figure 1).

"central" kinetochore protein, as a fiducial marker, we still observed colocalization between kinetochore proteins (Figure 2). These data indicate that the characterized movements of single tagged kinetochore proteins in this assay likely represents entire kinetochore complexes.

In our assay, the mScarlet-I fluorophore used to tag proteins blinked on and off (Klementieva et al., 2017). Other red fluorescent protein tags tested, including mScarlet, TagRFP-T, and mRuby2, also blinked and/or bleached rapidly. From our single protein tagging (with GFP) experiments (Figure 1), we knew that Ndc80 and Mtw1 never disassociated from microtubules to which they were bound. Therefore, the patchy signal we saw with mScarlet-I fluorophore (Figure 2) was likely a result of our red fluorescent protein blinking on and off. This also meant that it was nearly impossible to draw any conclusions about kinetochore assembly on the microtubule at any single point in time (i.e., during lateral movement or the transition from lateral to end-on binding). But the colocalization of entire tracks over time in the kymographs, even with one reporter signal blinking, indicated that a multi-complex of kinetochore proteins was observed on microtubules in our assay.

Cryo-correlative light microscopy and electron tomography provides evidence that the reconstituted kinetochores are largely intact

Cryo-electron tomography (cryo-ET) is a powerful method for studying the structural organization of multi-protein complexes in their fully hydrated, native state (Schur, 2019). A challenge in cryo-ET is to relate specific protein localization to

the complex structural information that can be obtained with this method. To overcome this challenge and to test whether the kinetochore proteins in our reconstitution assay are indeed part of higher-order kinetochore assemblies, we established a cryo-correlative light microscopy and electron tomography procedure. In brief, samples were prepared from yeast cell lysates with GFP-labeled Spc105 and mRuby2-labeled Tub1 incubated with far-red MT seeds in a similar fashion to the TIRF assay (see Materials and Methods for details). Samples were vitrified and first imaged by cryo-fluorescence light microscopy to identify regions of interest for cryo-ET data collection (Figure 3a, c). The holey carbon film generated some fluorescent background in the GFP channel, but we could detect clear Spc105-GFP foci. These foci were then targeted for cryo-ET imaging. Large protein complexes associated with the lateral surface and the tip of individual microtubules were clearly visible in tomograms of these regions (Figure 3b, d; Supplemental Movies SV3, SV4). These approximately 100 nm long complexes are reminiscent of kinetochore particles assembled from purified yeast components (Gonen et al., 2012) (Figure 3b, d). Furthermore, our tomography data revealed electron densities that likely correspond to the Dam1 ring and the Ndc80 and MIND sub-complexes (Westermann et al., 2005; Jenni and Harrison, 2018; Ng et al., 2019) (Figure 3b, d). In combination with the co-localization data from the TIRF assay, our tomography data reinforces the conclusion that multi-protein kinetochore particles were present on yeast microtubules in our reconstitution cell lysate assays.

Torvi, JR. & Wong, J. *et al.* | Reconstituted Kinetochore Dynamics
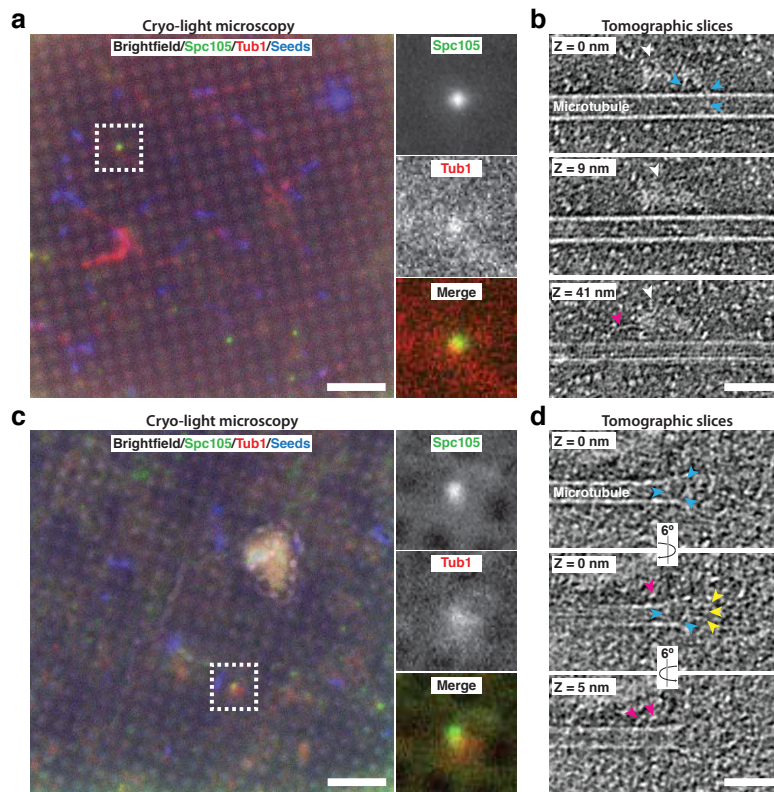
Figure 3. Cryo-correlative light microscopy and electron tomography shows microtubule-associated intact kinetochore complexes (**a**),(**c**) Overlay of brightfield and fluorescent channel cryo-light micrographs showing Spc105-GFP in green, mRuby-Tub1 in red and microtubule seeds in blue. The brightfield channel highlights the holey carbon film pattern. Insets show 2.7x magnified views of boxed regions. (b) Slices of tomogram recorded in the region of the highlighted Spc105 focus in (**a**) at Z-positions relative to the top slice. Slices show a kinetochore bound to the lateral surface of a microtubule. The largest part of the kinetochore appears as an electron-dense proteinaceous cloud similar to what has been reported for purified yeast kinetochores (white arrowheads; Gonen et al., 2012). A ring-like density (blue arrowheads) and a rod-like density (pink arrowheads), potentially representing Dam1 and Ndc80 sub-complexes, respectively, extend from the cloud-like density. (**d**) Slices of tomogram recorded in the region of the highlighted Spc105 focus in (**c**) at Z-positions relative to the top slice, showing a kinetochore complex bound to the end of a microtubule. Blue and pink arrowheads point at a ring-like (blue arrowheads) and rod-like (pink) density similar to the ones observed in (**b**) Additional rod-like extensions (yellow arrowheads) might represent the MIND complex. Scale bars, 10 μm in (**a,c**), 60 nm in (**b,d**).

## Kip3 is involved in kinetochore movement toward the microtubule plus end

After establishing that the kinetochore protein signals observed in our reconstitution assay represented intact kinetochore complexes, we began to probe the mechanism of the plus-end directed kinetochore movement. We postulated that the movement was driven by a kinesin motor protein. In budding yeast, there are only 5 kinesins, Kip2, Kip3, Cin8, Kip1, and Kar3 (Cottingham et al., 1999). To test the possibility that one of these motors was involved in kinetochore movement along microtubules in our assay, we systematically deleted each kinesin and asked whether kinetochore motility was impaired.

Upon deleting the genes encoding each of these motors, we found that only the highly processive plus-end directed kinesin-8, Kip3, was necessary for plus-end directed motility of the kinetochores (Figure 4a; Supplement Movie SV5). Specifically, 77% of laterally bound kinetochores moved in Kip3+ lysates compared to only 28% in *kip3Δ* lysates. Moreover, those laterally bound kinetochores that did move in *kip3Δ* lysates spent significantly less time moving toward the microtubule plus end compared to wild-type, and their run lengths were about half as far as those in Kip3+ lysates (0.46 μm vs 0.73 μm) (Figure 4b, c). Interestingly, although less frequent and covering shorter distances, kinetochore movements in *kip3Δ* lysates had the same velocity as the more frequent and

longer movements observed in Kip3+ lysates, moving at 0.47 μm/min (Figure 4d) (see Discussion).

Because the kinetochore movements in the *kip3Δ* lysate were relatively infrequent and covered short distances, only 5.7% of laterally bound kinetochores reached the plus end, compared to 28.1% in Kip3+ lysates. As in the Kip3+ lysates, when the kinetochore in the *kip3Δ* lysates was bound to the tip of the microtubule, depolymerization with the kinetochore tracking the microtubule plus end did occur. However, in this *kip3Δ* case, the microtubule plus ends with tip-bound kinetochores spent a significantly lower percentage of the time depolymerizing compared to what we observed in Kip3+ lysates (Figure 4b). This observation is consistent with a role for Kip3 in kinetochore-induced microtubule depolymerization (Gupta et al., 2006).

It was possible that, although Kip3 is required for kinetochore motility, that it in fact provided its essential function during kinetochore assembly. We therefore next tested whether providing a source of wild-type Kip3 to stationary kinetochores on microtubules assembled in *kip3Δ* lysates would enable those kinetochores to start to move. After observing immobile kinetochores on microtubules assembled in *kip3Δ* lysates for 10 minutes, lysate from a Kip3+ strain was added to the chamber. Immediately, these same stationary kinetochores began to move processively toward microtubule plus ends, establishing that Kip3 acts on previously assembled microtubule-bound kinetochores (Figure 4e). Therefore, the presence of func-
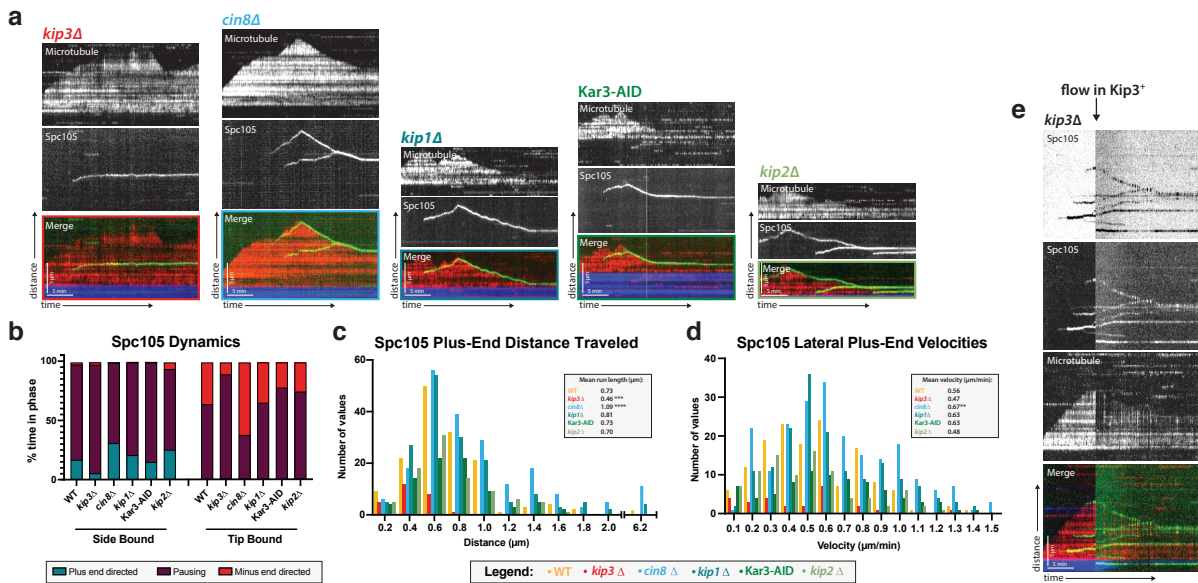
Figure 4. Kip3, a kinesin-8 motor, is required for plus-end directed movement of the kinetochore on the microtubule lattice (**a**) Genes encoding each of the five yeast kinesins were individually deleted (or the proteins degraded using a degron tag) and kinetochore dynamics on microtubules were assayed. Only Kip3, a highly processive kinesin-8, was required for kinetochore movement toward the microtubule plus end. Representative kymographs are shown with time on the x-axis and distance on the y-axis (scale bars are 5 min and 5μm, respectively). The kinetochore (Spc105) is shown in green and the microtubule is shown in red. The microtubule seed (at the minus-end of the growing red yeast microtubule) is shown in blue. (**b**) Quantification of dynamics over time shows that kinetochores in the *kip3Δ* strain spend the majority of the time paused, moving toward the plus end only 5% of the time compared to 30% for wild-type. (**c**) Run lengths and the number of runs the kinetochore made on the lattice toward the plus end were decreased in the *kip3Δ* strain. Run lengths were about half of wild-type, 0.46 μm vs 0.73 μm. The number of runs was also decreased to about 25% of the wild-type number of runs. Statistical analysis was done by a Kruskal-Wallis test where *** is P = 0.0001 and **** is P <0.0001. (**d**) Laterally bound kinetochores velocities are unchanged when moving in the plus end direction in a *kip3Δ* lysate. Statistical analysis was done using a Kruskal-Wallis test where ** is P = 0.0047. (**b-d**) Quantification is from 4 replicate trials of two biological replicates. For each strain from WT to *kip2Δ* lysate in the order listed, N = 128, 70, 129, 144, 103, 154 Spc105 proteins tracked. (**e**)Adding back a source of Kip3 to a lysate from a *kip3Δ* strain restores plus end-directed kinetochore movement. In lysates lacking Kip3, Spc105 (green) was immobile on the microtubule (red) surface. When Kip3+ lysate was added, the same, previously immobile, kinetochores started to translocate towards the microtubule plus ends.

tional Kip3 and/or its other binding partners was necessary for assembled kinetochores to translocate along the lateral surface of microtubules and not for kinetochore assembly or attachment to microtubules.

### Processive Kip3 transiently encounters slower moving kinetochores

We next set out to investigate the molecular mechanism by which Kip3 facilitates kinetochore plus end movement. To start, we asked whether we could observe Kip3 stably associated with moving kinetochores. To achieve this goal, we carried out dual-color imaging of the kinetochore (Spc105) and each of the motors assayed in the motor deletion screen described above. We observed Cin8 and Kip1 coming on and off the microtubule lattice stochastically at a high frequency, but they were not motile in our assay (Figure S2a). Kar3 was rarely observed on the microtubule (Figure S2a). For these three motors, anti-parallel or parallel bundled microtubules might be necessary to observe their previously reported activities in lysate (Su et al., 2013; Hepperla et al., 2014).

Of all the motors assayed, only Kip3 and Kip2 moved processively on the microtubule lattice (Figure 5; Figure S2a). However, kinetochore motility was only disrupted in *kip3Δ* lysates, not in *kip2Δ* lysates (Figure 4a-d). Therefore, processive motor movement towards the plus end alone is not sufficient to facilitate kinetochore movement along a microtubule. Kinetochore plus-end directed movement is dependent on Kip3 activity specifically. However, neither motor showed persistent colocalization with the kinetochores. The dual color tagging of Kip3 and Spc105 showed that there were brief moments of kinetochore movement where Kip3 signal

was observed running over or through the kinetochore signal (Figure 5c; Supplement Movie SV6)). Kip3 also moved much faster than either the speed of the kinetochore or the polymerization of the microtubule. However, Kip3 density on the microtubule was also very high and the bright signal might have obscured any Kip3 associated stably with kinetochores (see Discussion).

Kip3's tail domain is not needed for kinetochore motility, but Kip3's ability to attenuate microtubule dynamics is needed for kinetochores to reach the microtubule plus end

Comparison of *in vitro* and *in vivo* phenotypes of different Kip3 mutants might provide insights into the role of Kip3 in establishment of end-on attachments. In cells, knocking out the gene encoding Kip3 results in metaphase kinetochores that stay along the axis of the spindle, but are no longer focused into two discrete foci (Figure 5a & b) (Tytell and Sorger, 2006; Wargacki et al., 2010; Su et al., 2011). This declustered kinetochore phenotype has been proposed to be a result of improper spindle assembly and/or defective kinetochore-microtubule attachment (Shimogawa et al., 2010). Of interest to us was a Kip3 mutant, Kip3ΔT-LZ, that shows a declustered kinetochore phenotype *in vivo* (Figure 5a & b) (Su et al., 2011). In Kip3ΔT-LZ, the putative cargo-binding tail was truncated and replaced with a leucine zipper domain from Gcn4 transcription factor to restore dimerization of the motor heads (Su et al., 2011). Because the declustered chromosome phenotype *in vivo* is believed to be due to defects in kinetochore attachment, we hypothesized that, in our *in vitro* assay, we would observe laterally attached kinetochores in *kip3ΔT-LZ*

Torvi, JR. & Wong, J. *et al.* | Reconstituted Kinetochore Dynamics
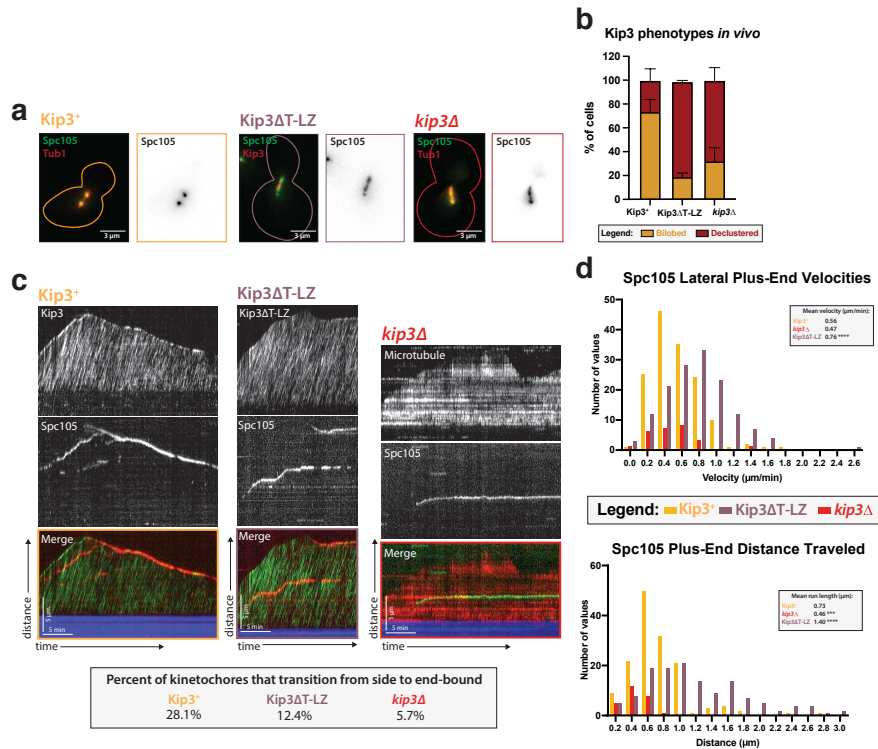
Figure 5. Kip3's motor activity, but not its depolymerase tail domain, is necessary for processive plus end-directed kinetochore movement (**a**) Metaphase cells with either wild-type Kip3, kip3Δ, or *kip3Δ T-LZ* alleles imaged in a *cdc23-1* strain expressing Spc105-GFP (green), mRuby-Tub1 or Kip3 (red). Note that the cells were not shifted to non-permissive temperature and were not arrested for imaging. Images are a maximum Z-projection of a 5μm stack of 0.2μm slices. (**b**) Quantification of the declustered kinetochore phenotype is shown as a bar graph for spindles that were 2-3 μm in length. Cells were classified as "bi-lobed" by a line scan showing two distinct peaks. The "declustered" phenotype included all line scans that did not show two peaks (line scans not shown). Two replicates were performed, each with n = 50 cells. Error bars are standard error of the mean. (**c**) Representative kymographs of Spc105 motility in wild-type, *kip3Δ T-LZ*, and *kip3Δ* lysates. Dual color tagging of wild-type Kip3 and Spc105 showed no clear colocalization between the kinetochore (red) and Kip3 (green). Kip3 is highly processive, moving much faster than the kinetochore. A Kip3 mutant containing a deletion in the tail region (Kip3ΔT-LZ, green) with the kinetochore (red) was still processive along the microtubule. The Kip3ΔT-LZ mutant showed robust processivity but it did not accumulate on microtubule plus ends and depolymerization events were fewer than in Kip3+ lysates, as shown in previously published literature. Lastly, a representative kymograph for *kip3Δ* lysate shows immobile Spc105 (green) on microtubules (red). (**d**) Histograms of Spc105 velocities and average run length when laterally bound and moving toward the microtubule plus ends. The number of values is shown on the y-axis and velocity/distance traveled on the x-axis, binned every 0.2 units. The mean velocity of wild-type Kip3 protein and Kip3ΔT-LZ protein is 0.55 μm/min and 0.76 μm/min, respectively. The average run length also increased from 0.73 μm to 1.4 μm. The mean Spc105 velocity in *kip3Δ* lysates was unchanged compared to wild-type, but the number of runs was reduced to 25% of wild-type. The average length decrease in *kip3Δ* was reduced from 0.73 μm to 0.45 μm. The mean is from 2 replicate trials of one biological replicate. Statistical analysis was done using a Kruskal-Wallis test where *** P = 0.0006 and **** P <0.0001. For lysates from each strain, as listed from WT to Kip3ΔT-LZ, N =128, 70, 81 kinetochores tracked.

lysates that do not become properly end-bound, similar to what we observed in *kip3Δ* lysates. Strikingly, in *kip3Δ T-LZ* lysates, kinetochores still moved processively toward the plus end of microtubules (Figure 5; Supplement Movie SV7). In fact, deleting the tail domain increased the velocity and the average run length of the kinetochore on the lattice of the microtubule (Figure 5d). In Kip3+ versus *kip3Δ T-LZ* lysate, the laterally bound plus end velocity increased from 0.56 μm/min to 0.76 μm/min and the average run length increased from 0.56 μm/min to 1.4 μm/min (Figure 5d).

As previously reported, the Kip3ΔT-LZ mutant protein did not accumulate on the plus ends of microtubules and it was unable to destabilize their plus ends and cause depolymerization (Su et al., 2011) (Figure S2b). Similarly, in a *kip3Δ* lysate, there was also altered microtubule dynamics, specifically a diminished catastrophe frequency (Bergman et al., 2018) (Figure S2b). Because of the reduced microtubule catastrophe frequency, we observed that in *kip3Δ T-LZ* lysates the kinetochore rarely reached the plus ends of polymerizing microtubules, despite it's faster velocity. Moreover, compared to the Kip3+ lysates where 28.1% of kinetochores transitioned from side to end-bound, only 12.4% of kinetochores made it to microtubule plus ends in *kip3Δ T-LZ* lysates. The increased

kinetochore lateral binding was even more dramatic in *kip3Δ* lysates, where only 5.7% of kinetochores transitioned from side- to end-bound (Figure 5c). These results indicate that the Kip3 tail domain is not required for kinetochore movement along microtubules, but is required for kinetochores to reach the plus end. Kip3's dual functions: (1) attenuation of kinetochore-microtubule dynamics, and (2) transport of kinetochores processively on the lattice, are needed for kinetochores to make end-on attachments. (see Discussion).

Discussion

Here we present a novel assay to follow kinetochore movement on microtubules in a cell free yeast system. We demonstrate that this assay allows individual kinetochores to be visualized while they are interacting with single microtubules. We observed kinetochore binding to microtubules, movement toward the microtubule plus end along the lattice, transition from side- to end-on attachment, apparently inducing depolymerization, and tracking of the depolymerizing end. Development of this kinetochore assay was achieved by adopting a previously established yeast extract system that allows analysis of dynamics of single yeast microtubules assembled in

the presence of the full complement of yeast proteins at defined cell cycle stages (Bergman et al., 2018). This assay involves native yeast proteins and allows us to combine the control over conditions provided by complementary powers of biochemistry and genetics to establish functions. We propose a model wherein kinetochores move to the microtubule plus ends powered by the budding yeast kinesin-8, Kip3. When kinetochores reach the microtubule plus ends, their attachments are converted to end-on attachments, at which point microtubule disassembly ensues (Figure 6).

Using both TIRF microscopy and cryo-electron tomography, we verified successful reconstitution of intact, microtubule-bound kinetochores. We observed nine different kinetochore proteins, spanning five kinetochore sub-complexes, and found that they all associate with and move along microtubules with similar dynamics (Figure 1a-e). The common behavior of these kinetochore proteins, combined with their colocalization with each other (Figure 2), indicated that complete or nearly complete kinetochore complexes were observed in the assay. Since our assay does not involve biochemical fractionation steps, and since the lysates retain the relative physiological concentration and ratio of soluble proteins, we were able to preserve the natural kinetochore composition (Biggins et al., 2013). Most importantly, by using cryo-correlative light-microscopy and electron tomography, we were able to directly visualize kinetochores bound to both the sides and ends of microtubules and found that their structures closely resemble negatively stained yeast kinetochores observed in earlier studies (Gonen et al., 2012). In both side- and end-bound arrangements, these kinetochore complexes included rod-like and ring-like structures that most likely are the Ndc80 complex and the Dam1 complex, respectively (Figure 3a-d) (Gonen et al., 2012; Westermann et al., 2005; Jenni and Harrison, 2018; Ng et al., 2019). Taken together, these observations establish that we were able to recapitulate dynamic kinetochore-microtubule binding in an *in vitro* single-molecule assay.

The ability to dynamically visualize individual reconstituted kinetochores on single microtubules made possible quantitative analysis of their dynamics along microtubules, which mimicked kinetochore behavior observed in spindles *in vivo* (Maiato et al., 2017). Kinetochores that bind to the side of the microtubule lattice move processively towards the plus end. Upon reaching the microtubule end, kinetochores convert their attachment to an end-bound conformation. During their conversion from lateral- to end-on attachment, and while bound to the microtubule end, kinetochores remain stably attached to the microtubule. Once bound to the microtubule ends, kinetochores track the tip of the depolymerizing microtubule. This transition to stable end-on attachments appeared to block microtubule polymerization and to induce depolymerization at a rate slower than the catastrophe rate for microtubules lacking kinetochores (Bergman et al., 2018) (Figure 1a-e). While tension stabilizes kinetochore-microtubule attachments on dynamic microtubules (Akiyoshi et al., 2010), in our presumably tension-less system, there was no observable kinetochore detachment from microtubule plus ends. Differences in kinetochore composition, cell cycle specific post-translational modifications, species-specific tubulin, buffer composition, or the presence of unidentified helper proteins could account for the differences. Notably, end-bound kinetochores do not normally detach from microtubules *in vivo* after attachment has been established during S phase (Tanaka et al., 2005). Additionally, in a previous *in vitro* study, chromosomes remained stably associated with depolymerizing microtubule ends (Koshland

et al., 1988). In the future, adapting our assay to include tension across the kinetochore promises to provide insights into how force impacts attachment and motility parameters. In summary, we were able to reconstitute intact kinetochores that associated with microtubule lateral surfaces and then underwent conversion to end-on attachment, which was followed by Anaphase A-like kinetochore-microtubule dynamics, with the kinetochores staying associated with depolymerizing microtubule plus ends.

Strikingly, reconstituted intact kinetochores associated with the lateral surface of dynamic microtubules stably, and they moved exclusively toward the plus end, and in a processive and kinesin-8-dependent manner. Kinetochores reached the plus end via a combination of directed movement and microtubule catastrophe. A role for Kip3, the budding yeast kinesin-8, in the translocation of kinetochores along microtubules is consistent with Kip3's reported *in vivo* colocalization with kinetochores and with its Ndc10-dependent association with centromeric DNA in ChIP assays (Tytell and Sorger, 2006). While our experiments did not show strong colocalization of Kip3 and kinetochores, it is possible that weak transient interactions are what facilitates kinetochore mobility via Kip3 (Figure 5c), or that low stoichiometry of Kip3 stably associated with kinetochores made detection impossible against a high background (Figure 5c) of free Kip3 molecules on the microtubules. Because our extract system uses undiluted soluble whole cell lysate, altering the Kip3 concentration to better observe a possible low-stoichiometry interaction between Kip3 and kinetochores was not possible. Additionally, quantification of kinetochore velocity on the microtubule lattice showed a wide distribution of rates punctuated by frequent pausing (Figure 1d-e). Both of these observations lend themselves to a model in which Kip3 affects kinetochore mobility in a stochastic way, perhaps by binding transiently. By this model, Kip3 sometimes moves the kinetochore in longer, faster runs, while other times, it displaces the kinetochore a short distance. Significantly, another processive microtubule-plus-end directed motor protein, Kip2 (Figure S2b), was insufficient to move kinetochores in *kip3Δ* lysates, which diminishes the possibility that non-specific collisions with the motor proteins are driving kinetochore translocation. The plus-end directed kinetochore motility we observed is specifically dependent on a processive Kip3 motor and was not dependent on this kinesin's tail domain.

Ideas & Speculation

We propose that Kip3 has a dual function in facilitating end-on attachment: (1) it attenuates kinetochore-microtubule dynamics to allow kinetochores to catch up with elongating microtubule plus ends, and it (2) moves kinetochores to the microtubule plus ends. Kinetochores did not move on microtubules in the *kip3Δ* lysate, but they did move in a highly processive manner in *kip3Δ T-LZ* lysates (Figure 5c-d). However, in lysates made from both Kip3 mutants (*kip3Δ* or *kip3Δ T-LZ*), we observed kinetochores that are laterally attached to microtubules, but these kinetochores rarely became end-bound. This observation can be explained if fewer kinetochores make it to the end of the microtubule. Specifically, in *kip3Δ* lysates, the inability to establish end-on attachments is likely largely due to a combination of impaired kinetochore motility and due to the microtubule dynamics being shifted toward more elongation with fewer catastrophes, making it less likely that kinetochores will reach microtubule plus ends (Figure 4a-d) (Figure S2b). In contrast, in *kip3Δ T-LZ* lysates the kinetochores are highly motile, but they establish end-on attachments less

Torvi, JR. & Wong, J. *et al.* | Reconstituted Kinetochore Dynamics
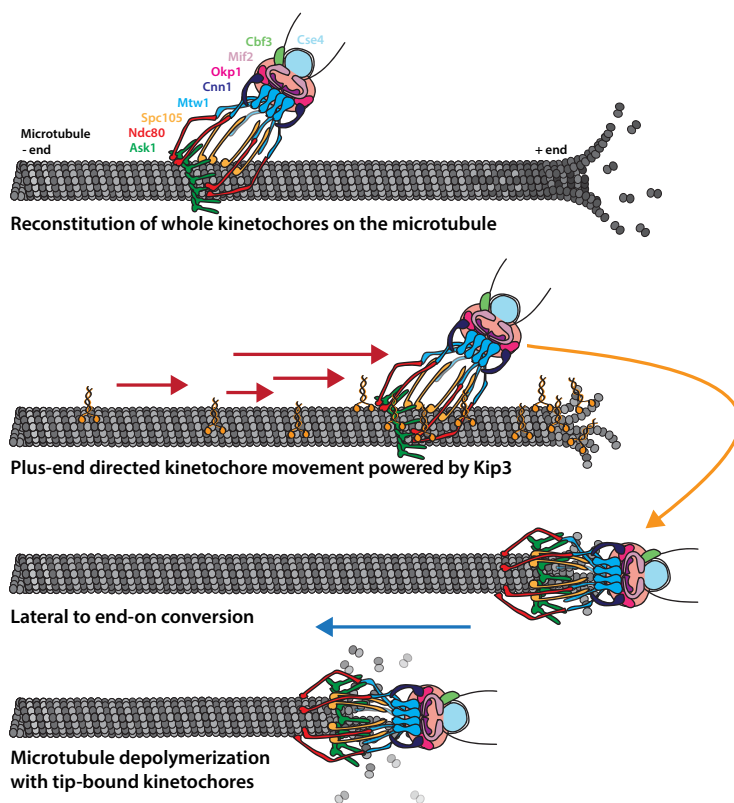
Figure 6. Cartoon model of reconstituted kinetochore dynamics on the microtubule Yeast kinetochores reconstituted binding with individual yeast microtubules in a yeast protein extract. These laterally-bound kinetochores travel in a directional manner to the plus end of the microtubule, powered by the kinesin-8, Kip3. Upon reaching the end of the microtubule, the kinetochore transitions to end-on attachment. Establishment of this end-on attachment coincides with onset of microtubule depolymerization and the end-bound kinetochore preventing the microtubule from elongating again.

frequently than in wild-type lysates. This result can be explained by the observations that the catastrophe frequency is severely diminished compared to wild-type microtubule dynamics, and that the microtubules mostly elongate faster than the rate of kinetochore translocation, so the kinetochores are less likely to encounter plus ends (Figure 5c-d) (Figure S2b).

It is useful to consider these *in vitro* results in the context of observations of kinetochore behavior in the corresponding mutant cells. In wild-type cells, sister chromatids are clustered in two foci within the metaphase spindle. In contrast, in *kip3Δ* cells metaphase kinetochores are declustered and aligned linearly along the spindle microtubules. This declustered kinetochore phenotype is also seen in *kip3Δ T-LZ* cells (Tytell and Sorger, 2006; Wargacki et al., 2010; Su et al., 2011) (Figure 5b). Based on the above *in vitro* and *in vivo* observations, we hypothesize that laterally bound kinetochores are an intermediate on the pathway toward biorientation, and that Kip3 is required for moving laterally attached kinetochores to the plus end of the microtubule during prometaphase. Specifically, we speculate that the previously reported declustered kinetochore phenotype is the result of an increased number of laterally bound kinetochores stalled all along spindle microtubules.

Methods

Yeast strains, culturing, and harvesting

Yeast strains used in this study can be found in Table S1. Fluorescent tagging, degradation tags, and deletions were integrated as previously described (Longtine et al., 1998; Lee et al., 2013; Bindels et al., 2017). All strains were grown in standard rich medium (YPD) at 25 °C since they contained a temperature-sensitive allele.

Cells were harvested as previously described in (Bergman et al., 2018). In brief, strains were grown overnight in starter cultures and then diluted back into two identical 2L cultures of YPD at an $OD600=6.25\times10^{-3}$. At an $OD600=0.4$ cultures were then shifted to 37 °C for a 3 hour arrest. Strains with degradation tags were treated with 250 μM 3-indole acetic acid (Sigma-Alrich, St. Louis, MO) in DMSO and 50 mM potassium phosphate buffer, pH 6.2, for 30 minutes before harvesting, 2.5 hours after the temperature shift. Cells were then harvested by serial centrifugation at 6000 x g in a Sorvall RC5B centrifuge using an SLA-3000 rotor for 10 minutes at 4 °C. Cell pellets were then resuspended in cold ddH2O and pelleted in a Hermle Z446K centrifuge for 3 mins at 3430 x g at 4 °C. This wash procedure was repeated once more, with any remaining liquid removed from the pellet via aspiration. Using a stainless steel lab spatula (Thermo Fisher, Waltham MA), the cells were then scraped out as small clumps into a 50 mL conical filled with liquid nitrogen, snap-freezing them, for storage at –80 °C.

Generation of whole cell lysates

As described previously by (Bergman et al., 2018), approximately 5g of frozen cells were weighed into a pre-chilled medium-sized SPEX 6870 freezer mill vial (Spex, Metuchen, NJ). The pre-chilled chamber was then milled (submerged in liquid nitrogen) following a protocol that consisted of a 3 minute pre-chill, then 10 cycles of 3 minutes grinding at 30 impacts per second (15 cps) and 1 minute of rest. The resulting powered lysate was stored at –80 °C.

Generating stabilized far-red labeled tubulin seeds

As previously described in (Bergman et al., 2018), purified bovine tubulin was cycled to remove nonfunctional tubulin. This tubulin was then mixed with both biotin-conjugated and HiLyte 647 labeled porcine tubulin (Cytoskeleton Inc., Denver, CO). The tubulin mix was then resuspended in PEM buffer (80 mM PIPES pH 6.9, 1 mM EGTA, 1 mM MgCl2) to a final concentration of 1.67 mg/mL unlabeled tubulin, 0.33 mg/mL biotin-labeled tubulin, and 0.33 mg/mL far-red labeled tubulin. To stabilize the seeds, GMPCPP (Jena Biosciences, Jena, Germany) was added to a final concentration of 1 mM. Aliquots were then snap-frozen in liquid nitrogen and stored at –80 ℃.

Preparation of glass sides and passivation of coverslips

Both glass side preparation and passivation of coverslips followed the protocol previously described in (Bergman et al., 2018). To prepare the glass sides for assembly into a flow chamber, microscope slides (Corning Inc., Corning, NY) were washed in acetone for 15 minutes and then 100% ethanol for 15 minutes. These slides were left to air dry before storage in an airtight container.

To prepare the coverslips for assembly into a flow chamber, cover glass (1.5 thickness, Corning Inc.) was first cleaned by sonication in acetone for 30 minutes. The coverslips were then soaked for 15 minutes in 100% ethanol. After 3 thorough, but short, rinses in ddH2O, the coverslips were submerged for 2 hours in 2% Hellmanex III solution (Hellma Analytics, Müllheim, Germany). After this, they were again rinsed in ddH2O three times. Before proceeding to passivation, the coverslips were blown dry with nitrogen gas. For passivation, a solution containing a 0.1 mg/mL mixture of PLL(20)-g[3.5]-PEG(2):PEG(3.4)-biotin(50%) (SuSoS AG, Dübendorf, Switzerland), at a ratio of 1:19, in 10 mM HEPES was prepared. 50 uL drops were then placed on Parafilm in a humid chamber and coverslips were gently placed onto the drops. After 1 hour, the passivated coverslips were washed for 2 minutes in PBS and rinsed in ddH2O for 1 minute. The coverslips were then air-dried with nitrogen gas and stored in an airtight container at 4 ℃. These passivated coverslips were stored for use only for three weeks.

Assembly of flow chamber

Preparation and assembly of the flow chamber for use in the TIRF based dynamics assay was exactly as described in (Bergman et al., 2018).

Preparation of whole cell lysates for dynamics assay

Similarly to what is described in (Bergman et al., 2018), 0.22 g of powdered lysate was weighed out into a 1.5 mL Eppendorf tube pre-chilled in liquid nitrogen. To assemble microtubules of a physiologically desired length (5 μm), a range of 1-25 μL of cold 10X PEM (800 mM PIPES pH 6.9, 10 mM MgCl2, 10 mM EGTA) was added to the powered lysate, as some strains required more or less buffer volumes to obtain 5 μm long microtubules in the assay. In addition to cold 10X PEM, 0.5 μL of Protease Inhibitor Cocktail IV (Calbiochem, San Diego, CA) and 4 μL of 25.5 U/μL benzonase nuclease (EMD Millipore, San Diego, CA, prod. 70746-3, >90% purity) was added, spun down briefly, and thawed on ice for 10 minutes. Lysate was added to pre-chilled polycarbonate ultracentrifuge tubes and cleared of insoluble material by spinning at 34,600 x g for 25 minutes at 4 ℃. After ultracentrifugation, 32 μL of cleared lysate supernatant was flowed into the chamber prepared previously (see above).

TIRF Microscopy

After clarified lysate supernatant was added to the prepared chamber, the slides were loaded onto a Nikon Ti2-E inverted microscope with an Oko Labs environmental chamber pre-warmed to 28 ℃. Images were acquired using a Nikon 60X CFI Apo TIRF objective (NA 1.49) and an Orca Fusion Gen III sCMOS camera (Hamamatsu, Hamamatsu City, Japan) at 1.5X magnification using the Nikon NIS Elements software. Using a LUNF 4-line laser launch (Nikon Instruments, Melville, NY) and an iLas2 TIRF/FRAP module (Gataca Systems, Massy, France) total internal reflection fluorescence (TIRF) illuminated a single focal plane of the field and was imaged every 5 seconds for 30 minutes.

Sequential lysate flow assays

Similar coverslip, slide, assembly of flow chamber, and lysate preparation were all followed as described above. However, instead of preparing one lysate for one genotype, two lysates were prepared side-by-side. To observe the initial behavior, 32 μL of the first lysate was flowed through the chamber and imaged for 10 minutes. While the slide was still mounted on the microscope, the video was paused for 1 minute while the second lysate was carefully flowed in, replacing the first. After replacing the lysate, the video was restarted and the same field of view was captured for another 20 minutes.

In vivo live cell microscopy

Cells were grown in rich medium (YPD) overnight to saturation at 25 ℃. The next day the cells were diluted into fresh YPD and grown for 4 hrs (2 doublings) at 25 ℃, until the culture reached log phase (OD600=0.5). They were then spun down and washed with minimal Imaging Medium three times (synthetic minimal medium supplemented with 20 μg/ml adenine, uracil, L-histidine and L-methionine; 30 μg/ml L-leucine and L-lysine; and 2% glucose; Sigma-Aldrich). Cells were then immobilized on coverslips coated with 0.2 mg/ml concanavalin A and were imaged in Imaging Medium. Using a Nikon Ti2-E inverted microscope with an Oko Labs environmental chamber pre-warmed to 25 ℃. Images were acquired with a Nikon 60X CFI Apo TIRF objective (NA 1.49) and an Orca Fusion Gen III sCMOS camera (Hamamatsu) at 1.5X magnification using the Nikon NIS Elements software. For imaging, a LUNF 4-line laser launch (Nikon) and an iLas2 TIRF/FRAP module (Gataca Systems) was used for HiLo total internal reflection fluorescence (Tokunaga et al., 2008). Images were taken with 0.2 μm slices for a total 5 μm Z-stack.

Image and data analysis

For the microtubule dynamics assay, analysis was done as described previously in (Bergman et al., 2018). Imaging data were analyzed using Fiji software (NIH). Registration to correct for stage drift was applied to the raw data (StackReg; (Thévenaz et al., 1998). Kymographs were generated from all microtubules for which the entire length could be tracked for the entire movie. Kymographs were excluded if the microtubules were crossed or bundled. For analysis, data from independent technical trials and biological replicas from one genotype were pooled, unless otherwise indicated. In our quantification of speeds, a minimum threshold of 86.7 nm/min for kinetochore movement rates was established based on the

resolution of the kymographs used to measure speed. Kinetochore movements less than a threshold slope of 1 pixel displacement (72.2 nm) per 10 pixels of time (50 sec) were categorized as "paused". Velocities are reported as mean with the standard error of the mean. Statistical significance was determined using a Kruskal-Wallis test (GraphPad Prism, San Diego, CA). P Values are reported as in the figure captions.

For the live cell imaging analysis, images were analyzed using Fiji (NIH). Maximum intensity Z-projections were made and bleach corrections were applied using the "histogram matching" macro. Metaphase cells were identified by the presence of a 2-3 µm spindle at the entrance to the bud neck. Cells were then counted as either "bilobed" or "declustered" based on the presence of two distinct kinetochore puncta. Line scans were done to assist in this binary classification. If two clear peaks were present, the cell was "bilobed." Any other line scan shape, i.e., 3+ peaks or 1 long kinetochore signal that matched the spindle, were classified as "declustered." Data are from two independent technical trials of one biological replicate. In each replicate, n = 50 cells were counted. Graphs are of the mean and standard error of the mean (GraphPad Prism).

Cryo-sample preparation

Holey carbon electron microscopy grids (Quantifoil R2/1, 200 mesh, copper; Electron Microscopy Science, Hatfield, PA) were washed in 99.5% acetone while agitating on a rocker for 15 to 30 min to remove potential residual plastic backing, then washed in H2O, and dried with filter paper. Cell lysate of DDY5818 (cdc23-1, SPC105-3xFlexLinker-yoEGFP, mRuby2-TUB1) strain was prepared as described above. After ultracentrifugation, supernatants were aliquoted into pre-chilled microcentrifuge tubes with a volume of 9.5 µL supernatant per aliquot and kept on ice. About 15 minutes before the lysate centrifugation was finished, far-red labeled GpCpp-stabilized MT seeds were polymerized in microcentrifuge tubes at 37 °C for 10 min. Grids were coated with 10 nm BSA Gold Tracer (Electron Microscopy Sciences) by dripping a total of 10 to 20 µL of the BSA Gold Tracer solution on the grids and removing the drops with filter paper. Seeds were diluted 1/50 in 1X PEM buffer. 0.5 µL of seeds were mixed with 9.5 µL cleared lysate. 3-6 µL of the mix were pipetted on the pre-coated grids. For sample vitrification, either a Vitrobot Mark IV (FEI, Hillsboro, OR) or a Leica EM GP2 (Leica Microsystems, Wetzlar, Germany) was used. Sample chamber conditions were set to 28 °C and 75-90% humidity. Samples were incubated in the sample chamber for 10-15 min and then blotted from the backside and vitrified by plunging into liquid ethane. To set up the Vitrobot Mark IV for back-blotting, the filter paper facing the sample side was replaced with a custom-made Teflon sheet of the same size to blot only the fluid from the back of the sample. To ensure that suitable grids were produced for each imaging session, a range of plot forces between 0 and 10 (for Vitrobot Mark IV only), blotting times of 3 to 6 s, and a 1 s drain time, were used. Grids were fixed into AutoGrid carriers (Thermo Fisher) and stored in liquid nitrogen until they were imaged.

Cryo-sample preparation

Cryo-samples were imaged on a Leica EM Cryo CLEM system (Leica Microsystems). The system consists of a Leica DM6 FS widefield microscope that is equipped with a motorized Leica EM Cryo stage and a short working distance (<0.28 mm) 50x Leica EM Cryo CLEM ceramic tipped objective (numerical aperture = 0.90). These specifications allow sample imaging at liquid nitrogen temperatures. A halogen lamp powered by a CTR6 halogen supply unit was used as a light source. We used GFP ET (Excitation: 470/40, Dichroic: 495, Emission 525/50), RFP (Excitation: 546/10, Dichroic: 560, Emission 585/40) and Y5 (Excitation: 620/60, Dichroic: 660, Emission 700/75) filter cubes for imaging. For cryo-correlative light and electron microscopy, a grid overview map was recorded using transmitted light and Y5 or GFP channels. The map was used to identify grid squares with good ice quality and intact carbon film. Z-stacks (total Z = 7 µm in 0.5 µm steps) of regions with clear fluorescence signals were recorded using the transmitted light, GFP (Spc105), RFP (Tub1) and Y5 (seeds) channels. These images were used to identify Spc105-GFP positive regions of interest for subsequent cryo-electron tomography imaging. The same imaging conditions were used for grid squares on individual grids. Imaging conditions were varied between grids to obtain sufficient signal to allow correlation in later steps. Images for panel generation in Adobe Illustrator were prepared using Fiji and Adobe Photoshop. No nonlinear gamma correction was applied during image processing.

Cryo-electron tomography data acquisition and tomogram reconstruction

Samples were imaged on a Titan Krios transmission electron microscope (FEI) equipped with an X-FEG electron source, a BioQuantum energy filter (Gatan, Pleasanton, CA) and a K3 direct electron detecting device (Gatan) and operated at 300 kV. Samples were visually inspected for ice quality using the FEI flu cam. Overview grid maps were acquired at 0.2 µm pixel size. These grid maps were used to identify grid squares of interest from the cryo-fluorescence light microscopy overview maps. Grid square images and polygon maps of the regions of interest with an overlap of 20-25% between individual images were recorded. The polygon maps were used to pick tilt series acquisition points based on the fluorescent signal from cryo-fluorescence light microscopy. The hole pattern of the carbon film was used as a guide. Acquisition points were chosen with adequate distance between individual points to prevent electron dose exposure damage prior to data collection. SerialEM (Mastronarde, 2005) in low-dose mode was used for automatic tilt-series recording using a bidirectional tilt scheme starting at +20° and with a typical tilt range from +60° to -60° and base increment of 2°. Pixel sizes between 2.63 and 3.07 Å were used. Target defocus was varied between -2 and -x µm and the targeted total electron dose was 100 e-/Å^2. Data were collected in 0.5 binning mode or without binning. Frame time was 0.2 – 0.25 s. Tilt series alignment and tomogram reconstruction were done using the freely available IMOD software package (Kremer et al., 1996). Tilt series were aligned using 10 nm gold particles as fiducials and tomograms were reconstructed using the backprojection algorithm combined with the SIRT-like filter. Tomograms were then filtered using the Nonlinear Anisotropic Diffusion filter and binned by a factor of 3 or 4 using the binvol function in IMOD to further increase contrast for analysis and visualization. Images for panel generation in Adobe Illustrator were prepared using IMOD and Adobe Photoshop. No nonlinear gamma correction was applied during image processing.

Acknowledgements

References

Akiyoshi, B., Sarangapani, K. K., Powers, A. F., Nelson, C. R., Reichow, S. L., Arellano-Santoyo, H., Gonen, T., Ranish, J. A., Asbury, C. L., and Biggins, S. Tension directly stabilizes reconstituted kinetochore-microtubule attachments. *Nature*, 468(7323):576–9, nov 2010. doi: 10.1038/nature09594.

Bergman, Z. J., Wong, J., Drubin, D. G., and Barnes, G. Microtubule dynamics regulation reconstituted in budding yeast lysates. *Journal of Cell Science*, 132:1–13, 2018. doi: 10.1242/jcs.219386.

Biggins, S., Gerring, S. L., Connelly, C., Hieter, P., and Dann, P. The composition, functions, and regulation of the budding yeast kinetochore. *Genetics*, 194(4):817–46, aug 2013. doi: 10.1534/genetics.112.145276.

Bindels, D. S., Haarbosch, L., Van Weeren, L., Postma, M., Wiese, K. E., Mastop, M., Aumonier, S., Gotthard, G., Royant, A., Hink, M. A., and Gadella, T. W. MScarlet: A bright monomeric red fluorescent protein for cellular imaging. *Nature Methods*, 14(1):53–56, 2017. doi: 10.1038/nmeth.4074.

Cheeseman, I. M., Chappie, J. S., Wilson-Kubalek, E. M., and Desai, A. The Conserved KMN Network Constitutes the Core Microtubule-Binding Site of the Kinetochore. *Cell*, 127(5):983–997, dec 2006. doi: 10.1016/j.cell.2006.09.039.

Ciferri, C., Musacchio, A., and Petrovic, A. The Ndc80 complex: Hub of kinetochore activity. *FEBS Letters*, 581(15):2862–2869, 2007. doi: 10.1016/j.febslet.2007.05.012.

Cottingham, F. R., Gheber, L., Miller, D. L., and Hoyt, M. A. Novel roles for Saccharomyces cerevisiae mitotic spindle motors. *Journal of Cell Biology*, 147(2):335–349, oct 1999. doi: 10.1083/jcb.147.2.335.

Craske, B. and Welburn, J. P. I. Leaving no-one behind : how CENP-E facilitates chromosome alignment. *Essays in Biochemistry*, 64:313–324, 2020. doi: https://doi.org/10.1042/EBC20190073.

Edzuka, T. and Goshima, G. Drosophila kinesin-8 stabilizes the kinetochore – microtubule interaction. *Journal of Cell Biology*, 218(2):474–488, 2019.

Fonseca, C. L., Malaby, H. L., Sepaniac, L. A., Martin, W., Byers, C., Czechanski, A., Messinger, D., Tang, M., Ohi, R., Reinholdt, L. G., and Stumpff, J. Mitotic chromosome alignment ensures mitotic fidelity by promoting interchromosomal compaction during anaphase. *Journal of Cell Biology*, 218(4): 1148–1163, 2019. doi: 10.1083/jcb.201807228.

Gestaut, D. R., Graczyk, B., Cooper, J., Widlund, P. O., Zelter, A., Wordeman, L., Asbury, C. L., and Davis, T. N. Phosphoregulation and depolymerization-driven movement of the Dam1 complex do not require ring formation. *Nature Cell Biology*, 10(4):407–414, 2008. doi: 10.1038/ncb1702.

Gonen, S., Akiyoshi, B., Iadanza, M. G., Shi, D., Duggan, N., Biggins, S., and Gonen, T. The structure of purified kinetochores reveals multiple microtubule-attachment sites. *Nature Structural Molecular Biology*, 19(9): 925–929, sep 2012. doi: 10.1038/nsmb.2358.

Goranov, A. I., Cook, M., Ricicova, M., Ben-Ari, G., Gonzalez, C., Hansen, C., Tyers, M., and Amon, A. The rate of cell growth is governed by cell cycle stage. *Genes and Development*, 23(12):1408–1422, 2009. doi: 10.1101/gad.1777309.

Grishchuk, E. L., Efremov, A. K., Volkov, V. A., Spiridonov, I. S., Gudimchuk, N., Westermann, S., Drubin, D. G., Barnes, G., McIntosh, J. R., and Ataullakhanov, F. I. The Dam1 ring binds microtubules strongly enough to be a processive as well as energy-efficient coupler for chromosome motion. *PNAS*, 105(40):15423–15428, 2008.

Gupta, M. L., Carvalho, P., Roof, D. M., and Pellman, D. Plus end-specific depolymerase activity of Kip3, a kinesin-8 protein, explains its role in positioning the yeast mitotic spindle. *Nature Cell Biology*, 8(9):913–923, sep 2006. doi: 10.1038/ncb1457.

Hepperla, A. J., Willey, P. T., Coombes, C. E., Schuster, B. M., Gerami-Nejad, M., McClellan, M., Mukherjee, S., Fox, J., Winey, M., Odde, D. J., O'Toole, E., and Gardner, M. K. Minus-end-directed kinesin-14 motors align antiparallel microtubules to control metaphase spindle length. *Developmental Cell*, 31 (1):61–72, oct 2014. doi: 10.1016/j.devcel.2014.07.023.

Irniger, S., Piatti, S., Michaelis, C., and Nasmyth, K. Genes involved in sister chromatid separation are needed for b-type cyclin proteolysis in budding yeast. *Cell*, 81(2):269–277, 1995. doi: 10.1016/0092-8674(95)90337-2.

Jenni, S. and Harrison, S. C. Structure of the DASH/Dam1 complex shows its role at the yeast kinetochore-microtubule interface. *Science*, 360(6388): 552–558, 2018. doi: 10.1126/science.aar6436.

Kalantzaki, M., Kitamura, E., Zhang, T., Mino, A., Novák, B., and Tanaka, T. U. Kinetochore-microtubule error correction is driven by differentially regulated interaction modes. *Nature Cell Biology*, 17(4):421–433, 2015. doi: 10.1038/ncb3128.

Kapoor, T. M., Lampson, M. A., Hergert, P., Cameron, L., Cimini, D., Salmon, E. D., McEwen, B. F., and Khodjakov, A. Chromosomes Can Congress to the Metaphase Plate Before Biorientation. *Science*, 311:388–392, 2006. doi: 10.1126/science.1122142.

Klementieva, N. V., Pavlikov, A. I., Moiseev, A. A., Bozhanova, N. G., Mishina, N. M., Lukyanov, S. A., Zagaynova, E. V., Lukyanov, K. A., and Mishin, A. S. Intrinsic blinking of red fluorescent proteins for super-resolution microscopy. *Chemical Communications*, 53(5):949–951, 2017. doi: 10.1039/c6cc09200d.

Koshland, D. E., Mitchison, T. J., and Kirschner, M. W. Polewards chromosome movement driven by microtubule depolymerization in vitro. *Nature*, 331(6156):499–504, 1988. doi: 10.1038/331499a0.

Kremer, J. R., Mastronarde, D. N., and McIntosh, J. R. Computer visualization of three-dimensional image data using IMOD. *Journal of Structural Biology*, 116(1):71–76, 1996. doi: 10.1006/jsbi.1996.0013.

Lee, S., Lim, W. A., and Thorn, K. S. Improved Blue, Green, and Red Fluorescent Protein Tagging Vectors for S. cerevisiae. *PLoS ONE*, 8(7):e67902, jul 2013. doi: 10.1371/journal.pone.0067902.

Lemura, K. and Tanaka, K. Chromokinesin Kid and kinetochore kinesin CENP-E differentially support chromosome congression without end-on attachment to microtubules. *Nature Communications*, 6, 2015. doi: 10.1038/ncomms7447.

Li, Y., Yu, W., Liang, Y., and Zhu, X. Kinetochore dynein generates a poleward pulling force to facilitate congression and full chromosome alignment. *Cell Research*, 17(8):701–712, 2007. doi: 10.1038/cr.2007.65.

Longtine, M. S., Mckenzie III, A., Demarini, D. J., Shah, N. G., Wach, A., Brachat, A., Philippsen, P., and Pringle, J. R. Additional modules for versatile and economical PCR-based gene deletion and modification in Saccharomyces cerevisiae. *Yeast*, 14(10):953–961, dec 1998. doi: 10.1002/(SICI)1097-0061(199807)14:10<953::AID-YEA293>3.0.CO;2-U.

Magidson, V., Paul, R., Yang, N., Ault, J. G., O'Connell, C. B., Tikhonenko, I., Mcewen, B. F., Mogilner, A., and Khodjakov, A. Adaptive changes in the kinetochore architecture facilitate proper spindle assembly. *Nature Cell Biology*, 17(9):1134–1144, 2015. doi: 10.1038/ncb3223.

Maiato, H., Gomes, A. M., Sousa, F., and Barisic, M. Mechanisms of chromosome congression during mitosis. *Biology*, 6(1):1–56, 2017. doi: 10.3390/biology6010013.

Mastronarde, D. N. Automated electron microscope tomography using robust prediction of specimen movements. *Journal of Structural Biology*, 152(1): 36–51, 2005. doi: 10.1016/j.jsb.2005.07.007.

Miranda, J. J., De Wulf, P., Sorger, P. K., and Harrison, S. C. The yeast DASH complex forms closed rings on microtubules. *Nature Structural and Molecular Biology*, 12(2):138–143, 2005. doi: 10.1038/nsmb896.

Ng, C. T., Deng, L., Chen, C., Lim, H. H., Shi, J., Surana, U., and Gan, L. Electron cryotomography analysis of Dam1C/DASH at the kinetochore-spindle interface in situ. *Journal of Cell Biology*, 218(2):455–473, feb 2019. doi: 10.1083/jcb.201809088.

Rieder, C. L. and Alexander, S. P. Kinetochores are transported poleward along a single astral microtubule during chromosome attachment to the spindle in newt lung cells. *Journal of Cell Biology*, 110(1):81–95, 1990. doi: 10.1083/jcb.110.1.81.

Risteski, P., Jagrić, M., Pavin, N., and Tolić, I. M. Biomechanics of chromosome alignment at the spindle midplane. *Current Biology*, 31(10):R574–R585, 2021. doi: 10.1016/j.cub.2021.03.082.

Schur, F. K. Toward high-resolution in situ structural biology with cryo-electron tomography and subtomogram averaging. *Current Opinion in Structural Biology*, 58:1–9, 2019. doi: 10.1016/j.sbi.2019.03.018.

Shimogawa, M. M., Wargacki, M. M., Muller, E. G., and Davis, T. N. Laterally attached kinetochores recruit the checkpoint protein Bub1, but satisfy the spindle checkpoint. *Cell Cycle*, 9(17):3619–3628, 2010. doi: 10.4161/cc.9.17.12907.

Stumpff, J., von Dassow, G., Wagenbach, M., Asbury, C. L., and Wordeman, L. The Kinesin-8 Motor Kif18A Suppresses Kinetochore Movements to Control Mitotic Chromosome Alignment. *Developmental Cell*, 14(2):252–262, feb 2008. doi: 10.1016/J.DEVCEL.2007.11.014.

Stumpff, J., Wagenbach, M., Franck, A., Asbury, C. L., and Wordeman, L. Kif18A and Chromokinesins Confine Centromere Movements via Micro-

tubule Growth Suppression and Spatial Control of Kinetochore Tension. *Developmental Cell*, 22(5):1017–1029, 2012. doi: 10.1016/j.devcel.2012.02.013.

Su, X., Qiu, W., Gupta, M. L., Pereira-Leal, J. B., Reck-Peterson, S. L., and Pellman, D. Mechanisms Underlying the Dual-Mode Regulation of Microtubule Dynamics by Kip3/Kinesin-8. *Molecular Cell*, 43(5):751–763, sep 2011. doi: 10.1016/j.molcel.2011.06.027.

Su, X., Arellano-Santoyo, H., Portran, D., Gaillard, J., Vantard, M., Thery, M., and Pellman, D. Microtubule-sliding activity of a kinesin-8 promotes spindle assembly and spindle-length control. *Nature Cell Biology*, 15(8):948–957, 2013. doi: 10.1038/ncb2801.

Tanaka, K., Mukae, N., Dewar, H., Van Breugel, M., James, E. K., Prescott, A. R., Antony, C., and Tanaka, T. U. Molecular mechanisms of kinetochore capture by spindle microtubules. *Nature*, 434:987–994, apr 2005. doi: 10.1038/nature03483.

Tanaka, T. U., Stark, M. J., and Tanaka, K. Kinetochore capture and bi-orientation on the mitotic spindle. *Nature Reviews Molecular Cell Biology*, 6(12):929–942, 2005. doi: 10.1038/nrm1764.

Tanaka, K. Dynamic regulation of kinetochore-microtubule interaction during mitosis. *Journal of Biochemistry*, 152(5):415–424, 2012. doi: 10.1093/jb/mvs109.

Tanaka, K. Regulatory mechanisms of kinetochore-microtubule interaction in mitosis. *Cellular and Molecular Life Sciences*, 70(4):559–579, 2013. doi: 10.1007/s00018-012-1057-7.

Thévenaz, P., Ruttimann, U. E., and Unser, M. A pyramid approach to subpixel registration based on intensity. *IEEE Transactions on Image Processing*, 7(1):27–41, 1998. doi: 10.1109/83.650848.

Tokunaga, M., Imamoto, N., and Sakata-Sogawa, K. Highly inclined thin illumination enables clear single-molecule imaging in cells. *Nature Methods*, 5(2):159–161, 2008. doi: 10.1038/NMETH.1171.

Tytell, J. D. and Sorger, P. K. Analysis of kinesin motor function at budding yeast kinetochores. *Journal of Cell Biology*, 172(6):861–874, 2006. doi: 10.1083/jcb.200509101.

Wargacki, M. M., Tay, J. C., Muller, E. G., Asbury, C. L., and Davis, T. N. Kip3, the yeast kinesin-8, is required for clustering of kinetochores at metaphase. *Cell Cycle*, 9(13):2581–2588, 2010. doi: 10.4161/cc.9.13.12076.

Weaver, B. A. and Cleveland, D. W. Decoding the links between mitosis, cancer, and chemotherapy: The mitotic checkpoint, adaptation, and cell death. *Cancer Cell*, 8(1):7–12, jul 2005. doi: 10.1016/j.ccr.2005.06.011.

Wei, R. R., Al-Bassam, J., and Harrison, S. C. The Ndc80/HEC1 complex is a contact point for kinetochore-microtubule attachment. *Nature Structural and Molecular Biology*, 14(1):54–59, 2007. doi: 10.1038/nsmb1186.

Westermann, S., Avila-Sakar, A., Wang, H. W., Niederstrasser, H., Wong, J., Drubin, D. G., Nogales, E., and Barnes, G. Formation of a dynamic kinetochore-microtubule interface through assembly of the Dam1 ring complex. *Molecular Cell*, 17(2):277–290, 2005. doi: 10.1016/j.molcel.2004.12.019.

Westermann, S., Drubin, D. G., and Barnes, G. Structures and Functions of Yeast Kinetochore Complexes. *Annual Review of Biochemistry*, 76(1):563–591, jun 2007. doi: 10.1146/annurev.biochem.76.052705.160607.

Supplementary Information
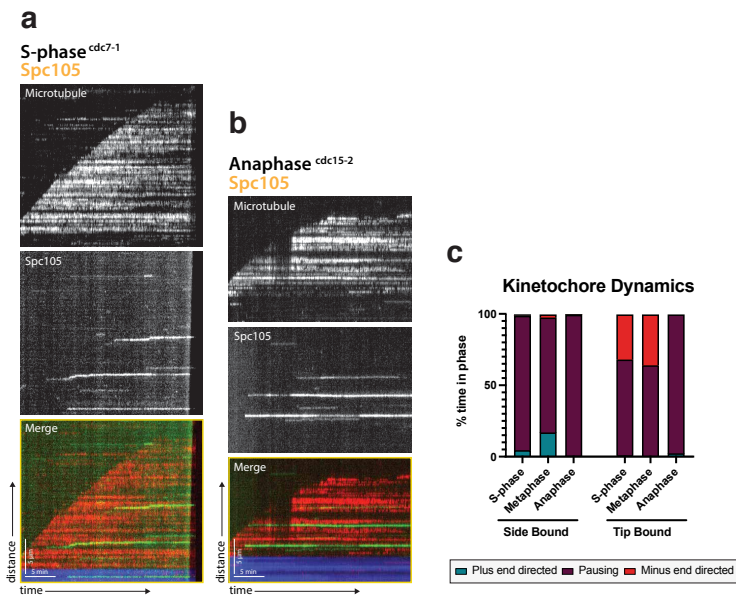
Figure S1. Kinetochore motility is specific to metaphase extracts (**a**) Representative kymograph from a S-phase arrested lysate (cdc7-1) with Spc105 (green) and the microtubule (red). (**b**) Representative kymograph from an anaphase arrested lysate (cdc15-2) with Spc105 (green) and the microtubule (red). (**c**) Kinetochore dynamics are shown by percent of time spent in each phase: plus-end directed, paused, or minus-end directed when either side bound or tip bound. S-phase and anaphase arrested kinetochore lysates spend the majority of the time paused on the lattice compared to metaphase.
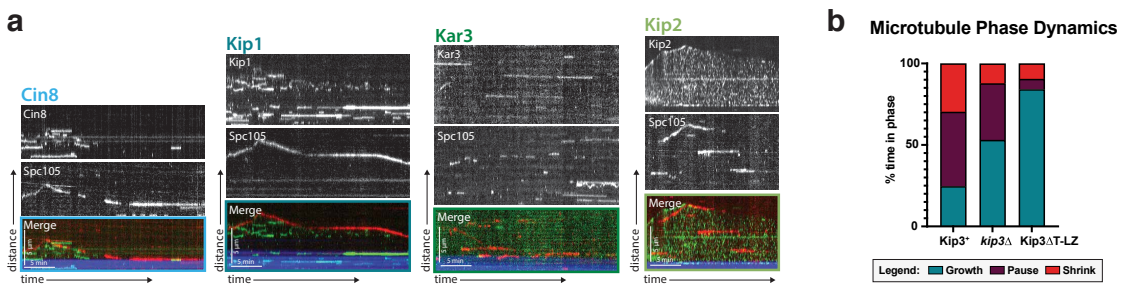
Figure S2. Kinetochores do no colocalize with the other four kinesins and Kip3's effect on microtubule dynamics (**a**) Dual color tagging of the kinetochore protein Spc105 and each of the five kinesins shows no clear colocalization. Representative kymographs are shown with the Spc105 in red and the kinesin motor proteins in green. The microtubule seed (minus-end) is in blue. (**b**) Across each of the three Kip3 conditions: wild-type, *kip3Δ*, and Kip3ΔT-LZ, the time the microtubule spent growing, shrinking, and paused changes. Wild-type Kip3 is the most dynamic, spending almost equal time in all three phases. The *kip3Δ* strain has an increased time spent paused and growing, while the Kip3ΔT-LZ strain spends the most time growing, rarely pausing or shrinking.

Supplementary Videos
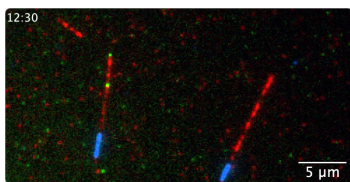
Figure SV1. Dynamic kinetochores on the microtubule
Spc105 (green) moves on the lattice of the microtubule (red) towards the plus-end. When reaching the tip, it transitions attachment and the microtubule begins to depolymerize, with the kinetochore tip-tracking. Scale bar is 5 µm. Frame rate is 20 frames per second.
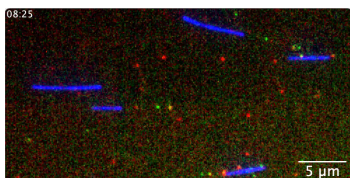

Figure SV2. Multiple kinetochore proteins are dynamic on the microtubule together
Mtw1 (red) colocalizes with Mif2 (green) and they move together in a directional manner. The microtubule is unlabeled due to experimental limitations of 4 color imaging, but, based on the data acquired when the microtubule could be imaged (Figure 1), kinetochore movement is on the lattice of the microtubule and moving towards the plus-end. When reaching the tip, the kinetochore transitions attachment and the microtubule begins to depolymerize, with the kinetochore tip-tracking. Scale bar is 5 µm. Frame rate is 20 frames per second.
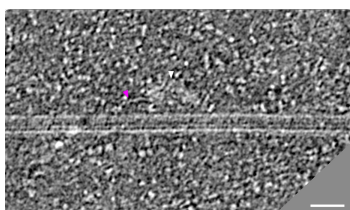

Figure SV3. Cryo-electron tomogram of kinetochore bound to the lateral surface of a microtubule
The largest part of the kinetochore appears as an electron-dense proteinaceous cloud (white arrowheads). A ring-like density (blue arrowheads) and a rod-like density (pink arrowheads), potentially representing Dam1 and Ndc80 sub-complexes, respectively, extend from the cloud-like density. Scale bar, 40 nm. Frame rate 20 frames per second.
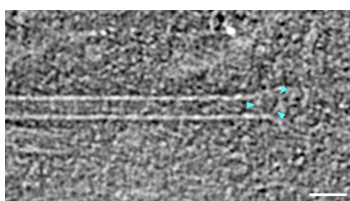

Figure SV4. Cryo-electron tomogram of kinetochore bound to the tip of a microtubule
Blue and pink arrowheads point at a ring-like (blue arrowheads) and rod-like (pink) density similar to the ones observed in Movie S3. Additional rod-like extensions (white arrowheads) might represent the MIND complex. Scale bar, 40 nm. Frame rate 10 frames per second.
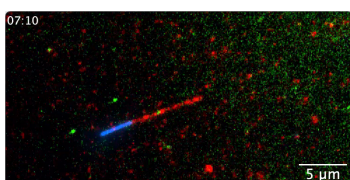

Figure SV5. Kinetochores do not move when the Kip3 gene is deleted
When Kip3 is deleted from the lysate, Spc105 (green) does not move on the lattice of the microtubule (red). The kinetochore is stationary on the microtubule. Scale bar is 5 µm. Frame rate is 20 frames per second.
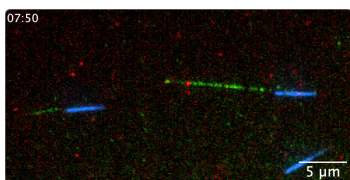
Figure SV6. Kinetochore and Kip3 dynamics
Spc105 (red) and Kip3 (green) move on the lattice of the microtubule towards the plus-end. Kip3 has short periods where it colocalizes and runs "through" the slow moving kinetochore. Scale bar is 5 µm. Frame rate is 20 frames per second.
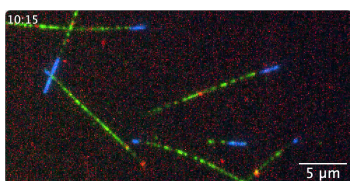
Figure SV7. Kinetochore and Kip3△T-LZ dynamics
Spc105 (red) and Kip3T-LZ (green) move on the lattice of the microtubule towards the plus-end. Kip3 has short periods where it colocalizes and runs "through" the slow moving kinetochore. Scale bar is 5 µm. Frame rate is 20 frames per second.